REGULAR ARTICLE

Theoretical design study on photophysical property of the organoboron quinolate derivatives

**Lu-Yi Zou · Ai-Min Ren · Xue-Qin Ran ·
Xue-Feng Ren · Ji-Kang Feng**

Abstract The photophysical properties of organoboron quinolate derivatives can be modified readily by manipulating the coordination environment around the central boron atom. This class of compounds applied in organic light-emitting diodes (OLEDs) materials has been studied by quantum chemistry. To reveal the relationship between the structures and properties of these electroluminescent materials, the ground- and excited-state geometries were optimized at the B3LYP/6-31G(d) and CIS/6-31G(d) levels, respectively. The ionization potentials and electron affinities were computed. The mobilities of hole and electron in these compounds were studied computationally based on the Marcus electron transfer theory. The maximum absorption and emission wavelengths of these compounds were calculated using the time-dependent density functional theory method. The solvent effect on the absorption and emission wavelengths of these compounds was also considered by a polarizable continuum model. These results show that boron compounds which containing both the hydroxyquinoline/hydroxybenzoquinoline as ligand and O/S in position X follow the rule, that is, the emission shifts to longer wavelength as covalent nature of the boron–ligand bonding is increased. Meanwhile, the negative HOMO and IPs decrease but the negative LUMO and EAs increase by substitution of O with S in position X.

It was deduced that both the hole- and electron-injection abilities are improved by substituting S in place of O in position X. After chemical modification in position R_2 with electron-donating properties of NH_2 or 1,4-diethynyl-2,5-dihexyloxybenzene, introduced 1,4-diethynyl-2,5-dihexyloxybenzene improves both the hole- and electron-transfer rate, which leads to better equilibrium property. It can be concluded that the better equilibrium property depends on the conjugated length of side chain in position R_2. Moreover, exchanging the substituents R_1 and R_2 in **BNO1a** and **BNO1'a** can slightly change the hole-transfer rate by 0.04 eV. According to these calculations, series **BNO** and **BNS** can be applied as electron transport and hole transport materials at the same time. Specially, series **BNO2** and **BNS** have better performance than $Mes_2B[p-4,4'-biphenyl-NPh(1-naphthyl)]$ (BNPB) in both the hole- and electron-injection ability.

1 Introduction

Since the discovery of a tris(8-hydroxyquinolinato)aluminum (Alq_3)-based multilayer thin-film device by Tang et al. [1], much progress has been made in organic electroluminescent (EL) devices. This phenomenon is attributed largely to the continuing discovery of new and improved EL materials. Most noteworthy was using the bis(10-hydroxybenzo[h]quinolinato) beryllium complex ($BeBq_2$) as an emitting material exhibits higher performance in EL properties than Alq_3, which was synthesized by Hamada et al. in 1993 [2]. Later, Wang et al. revealed that boron chelates in general are more stable than the corresponding

L.-Y. Zou · A.-M. Ren (✉) · X.-Q. Ran · X.-F. Ren ·
J.-K. Feng
State Key Laboratory of Theoretical and Computational
Chemistry, Institute of Theoretical Chemistry,
Jilin University, 130023 Changchun, China
e-mail: aimin.ren@gmail.com

J.-K. Feng
College of Chemistry, Jilin University,
130023 Changchun, China

aluminum chelates [3]. And these boron chelates exhibited various interesting properties due to the high electron affinity of boron atoms, strong fluorescence emission, good stability and volatility, easily gave a thin film, and third-order nonlinear optical properties, etc. Therefore, organoboron chelating ligands have received wide attention today [4–8]. Because of these unique properties, it is expected to design and synthesis of novel organoboron-based chelates materials with excellent optical and electrical properties. Theoretical study provides an essential role in developing materials [9, 10]. As in many recent publications in theoretical studies on organoboron chelates, much of what is mainly related to attachment of various substituents to the 8-hydroxyquinoline ligand. One of them achieved substitution at the 5 and the 7 positions of the quinolinolate were reported by our group. It is suggested that the styryl spacer between the quinoline ring and substituted phenyl ring extends the π-conjugated network, thus tuning the red-shift of absorption and emission spectra [11]. In this study, we continue to focus on the microcosmic mechanism of the luminescent properties for small boron chelates based on hydroxyquinoline, series **a** in Fig. 1, and finding an effective way to tune their optoelectronic properties.
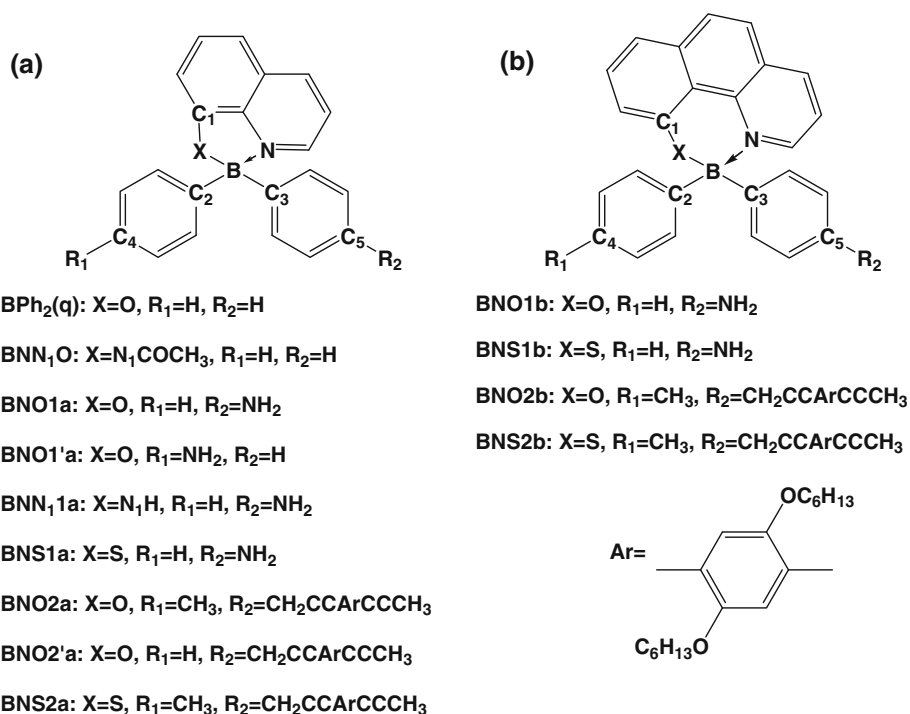
However, owing to BeBq$_2$ showing excellent electron transport characteristic with high electron mobility, we introduce hydroxybenzoquinoline group to the boron center (named series **b**). It is known in metal chelates of 8-hydroxyquinoline that as the covalent nature of the metal–ligand bonding is increased, the emission shifts to longer wavelength [12]. Chujo et al. revealed that

the low-molecular-mass organoboron quinoline-8-thiolate and -selenolate complexes are following this rule [4]. Although it can be concluded that series **a** will follow this rule after position X is substituted with O or S, the application of this rule to series **b** has not yet been investigated. Meanwhile, how to influence the color of fluorescent and the abilities of charge injection/transport via tuning position X with O, N or S and position R_2 with NH$_2$ or 1,4-diethynyl-2,5-dihexyloxybenzene and reveal which is the more sensitive site between R_1 and R_2 will be discussed in detail in this work.

2 Computation methods

To rationalize the experimentally observed properties of known materials and to predict those of unknown ones, theoretical investigations on the structures, electronic spectra, and emissive properties of these materials are indispensable, especially of some parameters, such as the ionization potential (IP), electron affinity (EA), and reorganization energies (λ), which are difficult to be obtained from experiments. Thus, we apply the density functional theory (DFT), configuration interaction with single excitations (CIS), and time-dependent DFT (TD-DFT) methods to investigate the geometrical structures and optical properties of these compounds such as the highest occupied orbital energies (HOMO), the lowest virtual orbital energies (LUMO), $\Delta_{H–L}$ (the energies difference between the HOMO and LUMO), IPs, EAs, λ, and the absorption and

Fig. 1 Sketch map of the structures for the studied systems

(a)

BPh$_2$(q): X=O, R$_1$=H, R$_2$=H

BNN$_1$O: X=N$_1$COCH$_3$, R$_1$=H, R$_2$=H

BNO1a: X=O, R$_1$=H, R$_2$=NH$_2$

BNO1'a: X=O, R$_1$=NH$_2$, R$_2$=H

BNN$_1$1a: X=N$_1$H, R$_1$=H, R$_2$=NH$_2$

BNS1a: X=S, R$_1$=H, R$_2$=NH$_2$

BNO2a: X=O, R$_1$=CH$_3$, R$_2$=CH$_2$CCArCCCH$_3$

BNO2'a: X=O, R$_1$=H, R$_2$=CH$_2$CCArCCCH$_3$

BNS2a: X=S, R$_1$=CH$_3$, R$_2$=CH$_2$CCArCCCH$_3$

(b)

BNO1b: X=O, R$_1$=H, R$_2$=NH$_2$

BNS1b: X=S, R$_1$=H, R$_2$=NH$_2$

BNO2b: X=O, R$_1$=CH$_3$, R$_2$=CH$_2$CCArCCCH$_3$

BNS2b: X=S, R$_1$=CH$_3$, R$_2$=CH$_2$CCArCCCH$_3$

Ar=

OC$_6$H$_{13}$

C$_6$H$_{13}$O

Table 1 Selected important bond lengths (Å), bond angles (°) and dihedral angles (°) of these compounds obtained by B3LYP/6-31G(d) calculations

	BPh$_2$(q)	BNN$_1$O	BNO1a	BNO1'a	BNN$_1$1a	BNO1b	BNO2a	BNO2'a	BNO2b	BNS1a	BNS1b	BNS2a	BNS2b
C$_1$–X(O/N$_1$/S)	1.325	1.393	1.324	1.324	1.351	1.330	1.325	1.326	1.332	1.744	1.757	1.745	1.758
X(O/N$_1$/S)–B	1.530	1.598/1.587[a]	1.533	1.534	1.569	1.491	1.530	1.529	1.487	2.013	1.942	2.006	1.939
B–N	1.658	1.637/1.619[a]	1.662	1.664	1.649	1.659	1.658	1.656	1.658	1.628	1.646	1.625	1.643
B–C$_2$	1.612	1.624/1.606[a]	1.615	1.607	1.622	1.617	1.609	1.611	1.614	1.619	1.622	1.614	1.620
B–C$_3$	1.614	1.625/1.611[a]	1.605	1.613	1.619	1.621	1.614	1.614	1.626	1.609	1.619	1.614	1.623
C$_4$–R$_1$	1.087	1.087	1.087	1.402	1.087	1.088	1.511	1.087	1.511	1.087	1.087	1.511	1.511
C$_5$–R$_2$	1.087	1.087	1.402	1.087	1.403	1.404	1.423	1.423	1.423	1.402	1.404	1.423	1.423
C$_1$–X(O/N$_1$/S)–B	111.57	111.46	111.68	111.74	113.86	120.98	111.56	111.51	121.02	93.26	99.26	93.04	99.28
X(O/N$_1$/S)–B–C$_2$	111.35	113.38/113.37[a]	110.73	111.70	113.63	108.14	111.45	111.49	108.50	112.65	106.38	113.16	106.77
X(O/N$_1$/S)–B–N	97.84	96.16/96.07[a]	97.60	97.51	95.25	105.14	97.86	97.94	105.24	98.68	104.11	98.96	104.34
N–B–C$_3$	109.85	108.12/107.68[a]	108.41	107.77	110.07	107.16	109.74	109.92	106.98	109.80	106.79	109.70	107.03
C$_2$–B–C$_3$	117.10	117.61/114.9[a]	117.27	117.44	115.75	115.96	117.07	116.86	115.49	116.63	115.31	116.34	114.70
N–B–C$_2$–X(O/N$_1$/S)	106.33	104.17	106.53	106.90	104.15	113.66	106.52	106.58	114.15	107.99	112.56	108.93	113.15
N–B–C$_3$–X(O/N$_1$/S)	107.05	105.16	106.29	105.63	104.81	114.36	106.91	107.13	114.32	107.28	113.83	107.09	114.03
C$_1$–X(O/N$_1$/S)–B–N	0.50	2.96	0.69	1.04	3.39	43.01	0.95	0.98	42.86	4.05	50.99	6.65	50.80

[a] The experimental values were subjected to X-ray diffraction study [5]

emission spectra are obtained and discussed in detail. The polarizable continuum model (PCM) was used in calculation of the absorption and emission spectra in CH$_2$Cl$_2$. All calculations of the studied organoboron quinolate derivatives in this work have been performed on the SGI origin 2000 server using the Gaussian03 program package [13]. And all the calculations were performed using the 6-31G(d) basis set.

3 Results and discussion

3.1 Geometry optimization

The sketch map of the structures is depicted in Fig. 1. From Fig. 1, it was found that the hydroxyquinoline group in system **a** is chelated to the boron to form a five-membered chelate ring. And the hydroxybenzoquinoline group in system **b** is chelated to the boron in the same manner to form a six-membered chelate ring. This difference between five- and six-membered chelate ring will cause dramatic difference in properties of the studied compounds. Furthermore, the nature of our studied chelates is also dominated by position X or R$_2$.

To provide an insight into the structure–property relationship of these compounds, we optimized the neutral ground-state structures at the DFT//B3LYP/6-31G(d) level of theory [14]. Selected important bond lengths, bond angles, and dihedral angles are listed in Table 1, compared with data from experimental values. As shown in Table 1, these results are in good agreement with experimental values. This indicates that our adopted method is feasible

to the studied systems. Comparison has been made between systems **1** and **2**. The substitution of R$_2$ with the group of 1,4-diethynyl-2,5-dihexyloxybenzene leads to a decrease in the B–N bond length (from 0.001 to 0.004 Å) for system **2** compared with system **1**, which might increase the chelating ability. It is because that the coordination bond plays an important role in the stability of the chelate, which is usual to initially determine the chelating ability. By substitution of O with N in position X, the bond length of B–N in both **BNN$_1$O** and **BNN1a** is shortened relative to that in **BPh$_2$(q)** and **BNO1a**. Upon decreasing atomic electronegativity in position X, the B–N bond length of **BNO1a**, **BNN$_1$1a** and **BNS1a** is gradually shortened. Comparison of the chelates formed with O or S, the bond length of B–N in series **BNS** is shorter (from 0.013 to 0.034 Å) than that in series **BNO**. These results suggested that the shortened bond length of B–N probably enhances the ability of chelating, which will benefit the ability of charge injection. Furthermore, previous studies have reported that as the covalent nature of the metal–ligand bonding (primarily metal-nitrogen) is increased, the emission shifts to longer wavelength [12]. Features are similar in some respects between boron chelates and metal chelates. We predict that the emissions in series **BNS** are red-shifted compared with that of series **BNO**. Meanwhile, there are other significant changes that occur in the geometries as a result of replacing the hydroxyquinoline group and O atom with hydroxybenzoquinoline group and S atom. Compared to system **a**, there are both bigger bond angle (X–B–N) and dihedral angle (C$_1$–X–B–N) in system **b** owing to the hydroxybenzoquinoline group. This result enhances the steric hindrance around the central B atom. The strength of B–N

bond in series **BNSb** is weakened obviously by the steric
hindrance, which is assisted by the presence of steric hin-
drance in Mq_3 (M = Al, Ga. In) chelates for effecting
change in the M–N bond [12]. Because of similar features
with metal (Al, Ga. In) chelates, it indicates that the
emission spectra will be red-shifted in series **BNSa** relative
to that of series **BNSb**. The sp^3 orbital-hybridized boron
centers of series **b** appear as a distorted tetrahedron with
dihedral angle of C_1–X–B–N > 42°, but series **a** has better
syn-planar conformation (C_1–X–B–N < 7°). It can be
concluded that series **a** shows better fluorescence proper-
ties. Otherwise, there are slight differences in the structures
between **BNO1a** and **BNO1'a**, and **BNO2a** and **BNO2'a**.
The bond length of B–N in **BNS2a** is shorter than others,
implying that **BNS2a** has better charge-injection ability
than others. Interestingly, the B–N bond length of **BNO2a**
is equal to that of **BNO2b**.

3.2 Frontier molecular orbitals

Since the relative ordering of the occupied and virtual
orbitals provides a reasonable qualitative indication of the
excitation properties [15] and of the ability of electron or
hole transport, it is important to analyze the HOMOs and
the LUMOs for these compounds. In this section, the
HOMOs and LUMOs of these compounds are investigated
at B3LYP/6-31G(d) level, and the orbital plots are present
in Fig. 2. As shown in Fig. 2, these molecules display a
tetrahedral structure, typical of boron compounds. The
hydroxyquinoline group has the largest contribution to both
the HOMO and LUMO in **BPh₂(q)** and **BNN₁O** without
any substitute in position R_1 or R_2. So, the chelating ability
of **BPh₂(q)** and **BNN₁O** will have influence on both the
hole- and electron-injection ability. Following the order
of **BNN₁a**, **BNS1a** and **BNO1a**, the HOMO level in
BNN₁a, **BNS1a** and **BNO1a** will be gradually lower with
the smaller HOMO contributions. Furthermore, the HOMO
and LUMO contributions in series **BNO** and **BNS** are
mainly located on the electron-rich R_2 group and the
electron-deficient hydroxyquinoline or hydroxybenzoquin-
oline group, respectively. The energy transfer from the π-
conjugated linkers in the main chain to the quinoline
ligands on the boron centers is attributed to the electron
push–pull effect of substitutes. Replacing O with S in series
BNS has larger contributions to both the HOMO and
LUMO than that in series **BNO**, which can improve the
hole- and electron-injection ability.

The HOMO and LUMO energies are experimentally
estimated from an empirical formula proposed by Brédas
et al. [16] based on the onset of the oxidation and reduction
peaks measured by cyclic voltammetry [17]. The hole and
electron injection of the materials is usually estimated by
the values of HOMO and LUMO, in accord with the work

function values of cathode and anode. The hole transport
material (HTM) with the smaller negative value of HOMO
should lose their electrons more easily, while the electron
transport material (ETM) with larger negative value of
LUMO should accept electrons more easily. The HOMO
and LUMO energies were calculated by DFT in this study.
The HOMO and LUMO energies and energy difference
Δ_{H-L}s of these compounds are listed in Table 2.

It can be seen from Table 2 that the HOMO levels of
these compounds match well with the work function of the
Indium Tin Oxides (ITO; from −4.8 to −5.1 eV) [18],
except **BPh₂(q)** and **BNN₁O**. This implies that these
compounds are promising as HTM, which depends on the
side chain of position R with electron-donating substitu-
tion. Furthermore, organoboron quinolate derivatives were
usually used to act as ETM. According to the LUMO
values, our studied compounds exhibit more excellent ET
properties than that of Alq_3 (LUMO, −1.81 eV), one of
most widely used electron transport materials [1, 19].
Therefore, series **BNO** and **BNS** and **BNN₁a** may act as
bifunctional (HT and ET) molecular OLEDs. Among
them, the hole- and electron-injection ability in **BNN₁a**
is higher (−4.88 eV) and lower (−1.87 eV) than others,
respectively.

Comparison of these HOMO and LUMO values,
BNN₁O has better hole- and electron-injection ability than
that of **BPh₂(q)**. The hole-injection ability is reduced
gradually in the order of **BNN₁a**, **BNS1a** and **BNO1a**.
Both the hole- and electron-injection ability of series **BNS**
are enhanced after replacing O with S in position X. These
results are consistent with the prediction made by the
density distribution. Beside these results, series **b** with
hydroxybenzoquinoline group greatly enhances the hole-
injection ability but almost no effects on electron-injection
ability. Conversely, the lengthened conjugation of position
R_2 in series **2** improves electron-injection ability effec-
tively but the hole-injection ability slightly. It is indicating
that the extended coplanar conjugated conformation and
the lengthened conjugation of position R_2 can improve the
hole- and electron-injection ability, respectively. Thus, it
can be obtained a wide variety of useful OLEDs via tuning
the substitution in different position. In addition, compared
the HOMO and LUMO values of **BNO1a** and **BNO2a** with
BNO1'a and **BNO2'a**, there are minor changes in HOMO
and LUMO due to the same substitution in different posi-
tion and adding a methyl in position R_1, respectively. This
result confirms that the prediction from the ground-state
geometries is discussed earlier.

Noticeably, the energy gap of series **BNS** becomes
narrow after chemical modification of O with S, leading to
the emission wavelengths red-shifted. The narrower energy
gap in series **BNS** is easier to form excitons than that of
series **BNO**.
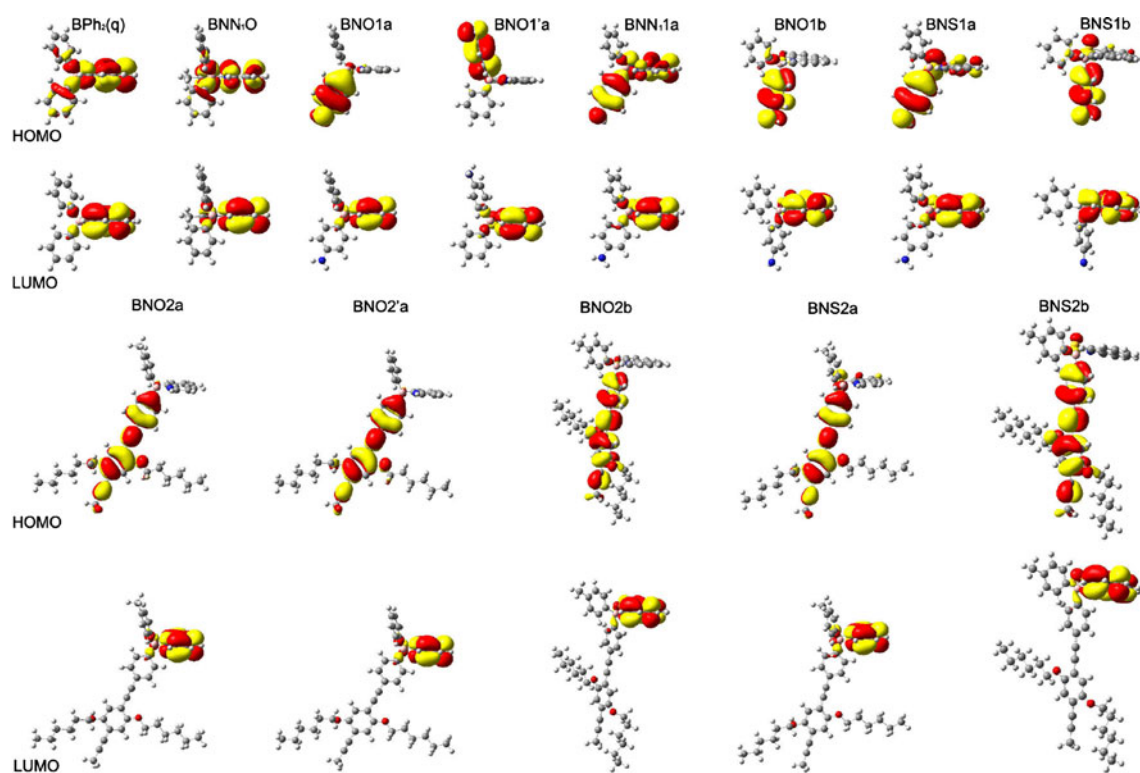
Fig. 2 Electronic density contours of the frontier orbitals for these compounds

Table 2 Negative value of the HOMO ($-\varepsilon_{HOMO}$) and LUMO ($-\varepsilon_{LUMO}$) energies, and HOMO-LUMO gaps calculated by B3LYP/6-31G(d)

	BPh$_2$(q)	BNN$_1$O	BNO1a	BNO1'a	BNN$_1$1a	BNO1b	BNO2a	BNO2'a	BNO2b	BNS1a	BNS1b	BNS2a	BNS2b
$-\varepsilon_{HOMO}$	5.73	5.65	5.07	5.06	4.88	4.93	5.01	5.02	4.94	4.95	4.91	4.96	4.92
$-\varepsilon_{LUMO}$	2.21	2.30	2.11	2.12	1.87	2.13	2.22	2.25	2.22	2.29	2.19	2.41	2.27
Δ_{H-L}	3.52	3.35	2.96	2.94	3.01	2.80	2.79	2.77	2.72	2.66	2.72	2.55	2.65

Unit: eV

3.3 Ionization potentials and electron affinities

The adequate and balanced transport of both injected electrons and holes are important in optimizing the performance of OLED devices. The ionization potential (IP) and electron affinity (EA) are well-defined properties that can be calculated by DFT to estimate the energy barrier for the injection of both holes and electrons into the compounds. Table 3 contains the calculated ionization potentials (IPs), electron affinities (EAs), both vertical (v; at the geometry of the neutral molecule) and adiabatic (a; optimized structure for both the neutral and charged molecule), and the extraction potentials (HEP and EEP for the hole and electron, respectively) that refer to the geometry of the ions [20, 21].

One general challenge for the application of small molecules in OLEDs is achievement of high EA-conjugated molecules for improving the electron injection/transport and low IP-conjugated molecules for better hole injection/transport in electronic devices. For an electroluminescent material, the lower the IP of the hole transport layer (HTL) itself, the easier will be the injection of holes from ITO to HTL, the higher the EA of the electron transport layer (ETL) itself, and easier the injection of electrons from cathode to ETL.

From Table 3, it is can be seen that the IP(a) and EA(a) values of series **b**, **2**, and **BNS** are lower and higher than that of series **a**, **1**, and **BNO**, respectively. This implies that both the hole- and electron-injection abilities are improved by the extended coplanar conjugated conformation, the lengthened conjugation of position R_2 and the enhanced electron-withdrawing in position X. Although it has been experimentally proved that 1,6-bis(2-hydroxyphenol)pyridinel boron bis(4-n-butyl-phenyl)phenyleneamine ((dppy)BTPA) (IP, 5.69 eV; EA, 0.80 eV) and BNPB (IP, 6.09 eV; EA, 0.74 eV) are good trifunctional molecules [22–25], the IP(a) and EA(a) values of series **BNO** and **BNS** are close to that of (dppy)BTPA and BNPB,

Table 3 Ionization potentials, electron affinities, extraction potentials and reorganization energies for each molecule

	IP(v)	IP(a)	HEP	EA(v)	EA(a)	EEP	λ_{hole}	$\lambda_{\text{electron}}$
BPh$_2$(q)	7.22	7.12	7.00	0.58	0.79	0.99	0.22	0.41
BNN$_1$O	7.11	6.97	6.81	0.74	0.94	1.13	0.30	0.39
BNO1a	6.68	6.35	5.98	0.48	0.71	0.92	0.70	0.44
BNO1'a	6.72	6.34	5.98	0.49	0.72	0.93	0.74	0.44
BNO1b	6.54	6.23	5.98	0.62	0.83	1.02	0.56	0.40
BNO2a	6.21	6.04	5.86	0.76	0.92	1.08	0.35	0.32
BNO2'a	6.23	6.07	5.89	0.77	0.93	1.10	0.34	0.33
BNO2b	6.13	5.99	5.83	0.83	0.98	1.15	0.30	0.32
BNS1a	6.40	6.10	5.77	0.73	0.92	1.11	0.63	0.38
BNS1b	6.37	6.01	5.65	0.73	0.92	1.10	0.72	0.37
BNS2a	6.07	5.94	5.79	0.96	1.11	1.27	0.28	0.31
BNS2b	6.06	5.90	5.73	0.89	1.06	1.25	0.33	0.36

Unit: eV

showing these compounds can be applied as both the HTL and ETL materials. According to the values of IP(a) and EA(a), series **BNO2** and **BNS** are easier to accept a hole and an electron than that of BNPB, implying that they exhibit more excellent properties as hole- and electron-injection materials than BNPB. In addition, the IP(a) and EA(a) values of **BNO1a** is 0.01 eV lower and higher than that of **BNO1'a**, respectively. The change trend of IP(a) and EA(a) for **BNO1a** and **BNO1'a** is equal to their negative of HOMO and LUMO energies. The IP(a) value of **BNO2a** with methyl in position R_1 is 0.03 eV lower than that of **BNO2'a**. It suggests that the methyl group in position R_1 can slightly improve the hole-injection ability. Therefore, series **2** with methyl group in position R_1 is further studied in the following section.

At the microscopic level, the charge-transport mechanism in thin film can be described as a self-exchange transfer process, in which an electron or hole transfer occurs from one charged molecule to an adjacent neutral molecule. The rate of intermolecular charge transfer (k_{et}) can be estimated from Marcus theory [26–28] given in

$$k_{\text{et}} = A \ \exp \left[\frac{-\lambda}{4k_b T} \right] \tag{1}$$

where T is the temperature, A is a prefactor related to the electronic coupling between adjacent molecules, λ is the reorganization energy and k_b is the Boltzmann constant. It will be seen that variations in the reorganization energies, which are exponential component (Eq. 1), dominate the changes in overall carrier transfer rates as the molecular structures are varied. For efficient charge transport, the reorganization energy requires to be small. At this stage, our discussion focuses on the reorganization energy.

The λ value is generally determined by fast changes in molecular geometry (the inner reorganization energy λ_i) and by slow variations in solvent polarization of the surrounding medium (the external contribution λ_e). In the case of LEDs (there are condensed-state systems), however, the latter contribution can be neglected, so that the former becomes the dominant factor. The inner reorganization energy λ_i for hole transfer can be expressed as follows:

$$\lambda_{\text{hole}} = \lambda_0 + \lambda_+ = \left(E_0^* - E_0 \right) + \left(E_+^* - E_+ \right) \tag{2}$$

where E_0 and E_+ represent the energies of the neutral and cation species in their lowest energy geometries, respectively, while E_0^* and E_+^* represent the energies of the neutral and cation species with the geometries of the cation and neutral species, respectively. In this way, $\lambda_{\text{electron}}$ for electron transfer can be expressed as follows:

$$\lambda_{\text{electron}} = \lambda_0 + \lambda_- = \left(E_0^* - E_0 \right) + \left(E_-^* - E_- \right) \tag{3}$$

The calculated λ_{hole} and $\lambda_{\text{electron}}$ are also listed in Table 3. As emitting-layer materials, they need to achieve balance between hole injection and electron acceptance. Furthermore, the lower the λ value, the higher the charge-transport rate. The data (Table 3) show that the difference between the λ_{hole} and $\lambda_{\text{electron}}$ for series **2** is less than 0.03 eV, implying that they can act as the emitter with relatively high light emitting efficiencies. So, series **2** has better transport equilibrium property than series **1**, which depends on the length of side chain. Exchanging the substituents R_1 and R_2 in **BNO1a** and **BNO1'a**, the λ_{hole} value of **BNO1a** is 0.04 eV lower than that of **BNO1'a**. This suggests that the hole-transfer rate is improved by position R_2 with NH$_2$. However, series **BNOb** with the increasing conjugated coplanar has better hole-transfer rate than that of series **BNOa**. Series **BNSa** with the increasing conjugated coplanar has better hole-transfer rate than that of series **BNSb**. It concludes that the hole-transfer rate in these compounds depend not only on the size of the coplanar conjugated conformation but also on the nature of the position X. Interestingly, both the $\lambda_{\text{electron}}$ and LUMO values of **BNO2a** are equal to that of **BNO2b**. The $\lambda_{\text{electron}}$ and LUMO and EA(a) values of **BNS2a** are smaller and higher than other compounds of our studied, respectively.
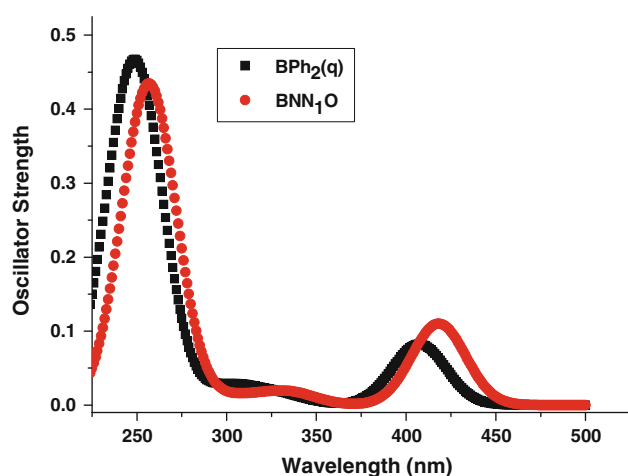
3.4 Absorption spectra and emission spectra

The transition energies, absorption spectra, oscillator strengths and main configurations for the most relevant singlet excited states in each molecule are listed in Table 4, accompanying with the experimental results. As shown in Table 4, S$_0$ → S$_1$ absorption peaks come from HOMO → LUMO $\pi\pi^*$ excitation. However, the strongest absorption peaks with the largest oscillator strength for these chelated

Table 4 Absorption spectra obtained by TD-DFT method for these molecules at the B3LYP/6-31G(d) optimized geometries

	Electronic transitions	λ_{max}^{abs} (nm)	f	Excitation energies (eV)	Main configurations	
BPh$_2$(q)	S$_0$ → S$_1$	426.2/395[a]	0.0605	2.91	HOMO → LUMO	0.66
	S$_0$ → S$_1$	407.3[b]	0.0824	3.04	HOMO → LUMO	0.66
	S$_0$ → S$_{12}$	245.1/242[a]	0.2460	5.06	HOMO-5 → LUMO	0.41
					HOMO-6 → LUMO	−0.33
					HOMO → LUMO + 1	0.21
					HOMO → LUMO + 2	−0.21
					HOMO-8 → LUMO + 1	0.14
					HOMO-2 → LUMO + 1	0.12
BNN$_1$O	S$_0$ → S$_1$	449.0/401[a]	0.0735	2.76	HOMO → LUMO	0.66
	S$_0$ → S$_1$	418.2[b]	0.1102	2.96	HOMO → LUMO	0.66
	S$_0$ → S$_{12}$	256.2	0.1113	4.84	HOMO → LUMO + 2	0.41
					HOMO-4 → LUMO + 1	−0.32
					HOMO-6 → LUMO	−0.23
					HOMO-1 → LUMO + 1	0.22
					HOMO-3 → LUMO + 1	0.18
					HOMO → LUMO + 3	0.10
BNO1a	S$_0$ → S$_1$	514.2	0.0012	2.41	HOMO → LUMO	0.70
	S$_0$ → S$_{10}$	261.6	0.0850	4.69	HOMO-6 → LUMO	0.56
					HOMO-5 → LUMO	−0.31
					HOMO → LUMO + 2	−0.16
BNO1ʹa	S$_0$ → S$_1$	517.4	0.0100	2.40	HOMO → LUMO	0.70
	S$_0$ → S$_{10}$	263.0	0.0790	4.72	HOMO-6 → LUMO	0.52
					HOMO-5 → LUMO	−0.38
					HOMO-3 → LUMO + 1	0.17
					HOMO → LUMO + 2	−0.12
BNO1b	S$_0$ → S$_1$	550.7	0.0022	2.25	HOMO → LUMO	0.70
	S$_0$ → S$_8$	313.4	0.0717	3.96	HOMO-5 → LUMO	0.63
					HOMO-1 → LUMO + 1	−0.17
BNO2a	S$_0$ → S$_1$	514.4	0.0026	2.41	HOMO → LUMO	0.70
	S$_0$ → S$_6$	351.7	1.2883	3.53	HOMO → LUMO + 1	0.63
					HOMO → LUMO + 2	0.11
BNO2ʹa	S$_0$ → S$_1$	517.7	0.0032	2.40	HOMO → LUMO	0.70
	S$_0$ → S$_6$	351.6	1.2448	3.53	HOMO → LUMO + 1	0.63
					HOMO → LUMO + 2	0.13
BNO2b	S$_0$ → S$_1$	530.2	0.0061	2.34	HOMO → LUMO	0.70
	S$_0$ → S$_7$	354.3	0.7271	3.50	HOMO-1 → LUMO + 1	0.48
					HOMO → LUMO + 2	0.44
					HOMO-8 → LUMO	0.11
BNS1a	S$_0$ → S$_1$	586.9	0.0219	2.11	HOMO → LUMO	0.69
	S$_0$ → S$_2$	491.5	0.0425	2.52	HOMO-1 → LUMO	0.67
BNS1b	S$_0$ → S$_1$	578.7	0.0019	2.14	HOMO → LUMO	0.70
	S$_0$ → S$_2$	483.5	0.0370	2.56	HOMO-1 → LUMO	0.67
BNS2a	S$_0$ → S$_1$	575.7	0.0316	2.15	HOMO → LUMO	0.69
	S$_0$ → S$_8$	353.9	1.0365	3.50	HOMO → LUMO + 2	0.55
					HOMO → LUMO + 1	−0.31
					HOMO-1 → LUMO + 2	0.16
BNS2b	S$_0$ → S$_1$	552.8	0.0023	2.24	HOMO → LUMO	0.69
					HOMO-1 → LUMO	−0.12
	S$_0$ → S$_8$	354.9	1.3513	3.49	HOMO → LUMO + 2	0.64

[a] Measured in CH$_2$Cl$_2$ [5, 8]

[b] Calculated in CH$_2$Cl$_2$ by PCM at the B3LYP/6-31G(d) level

Fig. 3 Simulated absorption spectra of **BPh₂(q)** and **BNN₁O** in CH₂Cl₂ with the calculated data at the TDDFT/B3LYP/6-31G(d) level

complexes are from the inner electronic transition. It was very similar to our previous study, which bound to the central B atom through N and O atoms [23]. The λ_{max}^{abs} of **BPh₂(q)**, **BNN₁O**, **BNO1a**, **BNO1b**, **BNO2a**, and **BNO2b** is red-shifted, which is in accord with the decrease in the HOMO-LUMO gaps. In addition, the influence of solvent CH₂Cl₂ on the absorption wavelengths of **BPh₂(q)** and **BNN₁O** is simulated at the B3LYP/6-31G(d) level using

the PCM, which is compared with those obtained from the gas phase. It can be seen that the coefficient and configurations have no change, but the absorption wavelengths have shifted (18.9 and 30.8 nm) and the oscillator strengths have increased (2.19 and 3.67%) in CH₂Cl₂ than that in the gas phase. More than that, the calculated absorption spectra of **BPh₂(q)** and **BNN₁O** in CH₂Cl₂ are in accordance with the experimental values, which are fitted by Gaussian type absorption curves and shown in Fig. 3. The shape of the calculated absorption spectra of **BNN₁O** in CH₂Cl₂ is the same as the spectra obtained by UV–vis absorption spectroscopy [5]. It indicates that our adopted basis set and functional are accurately reflected the optical and electronic properties.

As shown in Table 5, the calculated emission spectra of **BPh₂(q)** and **BNN₁O** in CH₂Cl₂ are in good agreement with the experimental values [5, 8]. The emission spectra in series **1**, **BNSa**, and **BNS** are red-shifted compared to that of series **2**, **BNSb** and **BNO**, respectively. Series **a** with larger oscillator strengths shows better fluorescence properties than that of series **b** due to the better syn-planar conformation, except **BNO2a**. These results are almost consistent with the ground-state geometries and the energy gap discussion above. Nevertheless, the vibrational relaxation is suppressed by enhanced the B–N chelating ability, series **BNS** has better fluorescence properties compared with series **BNO**. In addition, the B atom with the N and O

Table 5 Emission spectra obtained by TD-DFT method for these molecules at the CIS/6-31G(d) optimized geometries

	Electronic transitions	λ^{em} (nm)	f	Excitation energies (eV)	Main configurations	
BPh₂(q)	$S_1 \rightarrow S_0$	528.4/496[a]	0.0532	2.35	HOMO → LUMO	0.64
	$S_1 \rightarrow S_0$	505.8[b]	0.0722	2.45	HOMO → LUMO	0.65
BNN₁O	$S_1 \rightarrow S_0$	533.9/504[a]	0.0748	2.32	HOMO → LUMO	0.64
	$S_1 \rightarrow S_0$	502.1[b]	0.1091	2.47	HOMO → LUMO	0.65
BNO1a	$S_1 \rightarrow S_0$	564.6	0.0139	2.20	HOMO-1 → LUMO	0.69
BNO1'a	$S_1 \rightarrow S_0$	553.9	0.0036	2.24	HOMO → LUMO	0.69
					HOMO-1 → LUMO	−0.13
BNN₁1a	$S_1 \rightarrow S_0$	612.0	0.0511	2.03	HOMO → LUMO	0.64
BNO1b	$S_1 \rightarrow S_0$	568.8	0.0025	2.18	HOMO → LUMO	0.70
BNO2a	$S_1 \rightarrow S_0$	519.8	0.0001	2.39	HOMO → LUMO	0.70
BNO2'a	$S_1 \rightarrow S_0$	523.2	0.0001	2.37	HOMO → LUMO	0.70
BNO2b	$S_1 \rightarrow S_0$	551.7	0.0030	2.25	HOMO → LUMO	0.70
BNS1a	$S_1 \rightarrow S_0$	674.8	0.0421	1.84	HOMO → LUMO	0.67
BNS1b	$S_1 \rightarrow S_0$	666.6	0.0153	1.86	HOMO → LUMO	0.69
BNS2a	$S_1 \rightarrow S_0$	638.5	0.0665	1.94	HOMO → LUMO	0.69
					HOMO-1 → LUMO	0.14
BNS2b	$S_1 \rightarrow S_0$	599.7	0.0254	2.07	HOMO → LUMO	0.66
					HOMO-1 → LUMO	0.15

[a] Measured in CH₂Cl₂ [5, 8]

[b] Calculated in CH₂Cl₂ by PCM at the B3LYP/6-31G(d) level

atoms to form a six-membered chelate ring in series **b** has longer wavelengths than that of series **a**. In contrast, the boron compounds in series **a** chelated with the N and S atoms exhibited emission at longer wavelengths compared to that of series **b**. As the conjugation length of R_2 became larger, the more obvious variations occur in emission spectra. Based on the calculated emission spectra from 519.8 to 674.8 nm, we predict that these compounds could be used as green, yellow, orange and red light-emitting materials. In brief, their optoelectronic properties can be tuned by structural modifications in different positions with different substitutes.

4 Conclusions

In this study, the ground-state and excited-state properties of 13 compounds have been investigated using DFT, TDDFT and CIS methods, respectively. Ten of them have been predicted with multifunction. The better equilibrium property mainly depends on the conjugated length of side chain in position R_2. The λ_{hole} of these compounds depends not only on the size of the coplanar conjugated conformation but also on the nature of position X. The λ_{hole} of **BNO1a** is 0.04 eV lower than that of **BNO1'a**, due to the same substitution in different position, which can slightly change the hole-transfer rate. The absorption wavelengths in **BPh₂(q)**, **BNN₁O**, **BNO1a**, **BNO1b**, **BNO2a**, and **BNO2b** exhibit gradual red-shifts with the HOMO-LUMO gaps decreasing. The emission wavelengths of these compounds are located in green, yellow, orange and red range, implying that they can be used as green, yellow, orange and red light-emitting materials.

References

1. Tang CW, Van Slyke SA (1987) Appl Phys Lett 51:913
2. Hamada Y, Sano T, Fujita M, Fujii T, Nishio Y, Kenichi S (1993) Chem Lett 905–906
3. Wu Q, Esteghamatian M, Hu NX, Zoran P, Gary E, Steven RB, Wang S (1999) Angew Chem Int Ed Engl 38:985
4. Tokoro Y, Nagai A, Kokado K, Chujo Y (2009) Macromolecules 42:2988–2993
5. Nagata Y, Chujo Y (2008) Macromolecules 41:3488–3492
6. Nagata Y, Chujo Y (2007) Macromolecules 40:6–8
7. Rho HH, Jeong JH, Kim YK, Ha YK (2006) Current Applied Physics 6:712–717
8. Cui Y, Bai DR, Jia WL, Tao Y, Wang S (2005) Inorg Chem 44:601–609
9. Zou LY, Ren AM, Feng JK, Ran XQ, Liu YL, Sun CC (2008) J Phys Chem A 112:12172–12178
10. Zou LY, Zhang ZL, Ren AM, Ran XQ, Feng JK (2010) Theor Chem Acc 126:361–369
11. Li XN, Feng JK, Ren AM (2008) Chin J Chem 26:1979–1984
12. Chen CH, Shi J (1998) Coord Chem Rev 171:161–174
13. Frisch MJ, Trucks GW, Schlegel HB, Scuseria GE, Robb MA, Cheeseman JR, Montgomery JA Jr, Vreven T, Kudin KN, Burant JC, Millam JM, Iyengar SS, Tomasi J, Barone V, Mennucci B, Cossi M, Scalmani G, Rega N, Petersson GA, Nakatsuji H, Hada M, Ehara M, Toyota K, Fukuda R, Hasegawa J, Ishida M, Nakajima T, Honda Y, Kitao O, Nakai H, Klene M, Li X, Knox JE, Hratchian HP, Cross JB, Bakken V, Adamo C, Jaramillo J, Gomperts R, Stratmann RE, Yazyev O, Austin AJ, Cammi R, Pomelli C, Ochterski JW, Ayala PY, Morokuma K, Voth GA, Salvador P, Dannenberg JJ, Zakrzewski VG, Dapprich S, Daniels AD, Strain MC, Farkas O, Malick DK, Rabuck AD, Raghavachari K, Foresman JB, Ortiz JV, Cui Q, Baboul AG, Clifford S, Cioslowski J, Stefanov BB, Liu G, Liashenko A, Piskorz P, Komaromi I, Martin RL, Fox DJ, Keith T, Al-Laham MA, Peng CY, Nanayakkara A, Challacombe M, Gill PMW, Johnson B, Chen W, Wong MW, Gonzalez C, Pople JA (2004) Gaussian 03, revision C.02. Gaussian Inc., Wallingford, CT
14. Becke AD (1993) J Chem Phys 98(7):5648–5652
15. De Oliveira MA, Duarte HA, Pernaut JM, De Almeida WB (2000) J Phys Chem A 104:8256–8262
16. Brédas JL, Silbey R, Boudreaux DS, Chance RR (1983) J Am Chem Soc 105:6555–6559
17. Morisaki Y, Ishida T, Chujo Y (2003) Polym J 35:501
18. Huang CH, Li FY, Huang W (2005) The introduction for the organic light emitting materials and devices. Fudan University, Shanghai
19. Liu XD, Ren AM, Feng JK, Yang L, Xu H, Shi MM, Sun CC (2006) Chem J Chinese U 11:2156–2159
20. Curioni A, Boero M, Andreoni W (1998) Chem Phys Lett 294:263–271
21. Wang I, Botzung-Appert E, Stéphan O, Ibanez A, Baldeck PL (2002) J Opt A:Pure Appl Opt 4:S258–S260
22. Zhang H, Huo C, Zhang J, Zhang P, Tian W, Wang Y (2006) Chem Commun 3:281–283
23. Zou LY, Ren AM, Feng JK, Ran XQ, Liu YL, Sun CC (2009) Int J Quantum Chem 109:1419–1429
24. Jia WL, Feng XD, Bai DR, Lu ZH, Wang S, Vamvounis G (2005) Chem Mater 17:164–179
25. Zou LY, Ren AM, Feng JK, Ran XQ (2009) J Phys Org Chem 22:1104–1113
26. Marcus RA (1956) J Chem Phys 24:966–978
27. Marcus RA (1993) Rev Mod Phys 65:599
28. Liao Y, Yang GC, Feng JK, Shi LL, Yang SY, Yang L, Ren AM (2006) J Phys Chem A 110:13036